Environmental Science: Atmospheres

ROYAL SOCIETY OF CHEMISTRY

PAPER

View Article Online
View Journal | View Issue

Check for updates

Cite this: *Environ. Sci.: Atmos.*, 2022, **2**, 165

Received 1st July 2021
Accepted 22nd October 2021

DOI: 10.1039/d1ea00052g

rsc.li/esatmospheres

Emerging investigator series: the *red sky*: investigating the hurricane Ophelia Saharan dust and biomass burning aerosol event

Kevin P. Wyche, *[a] Hugo Ricketts, [bc] Mathew Brolly [a] and Kirsty L. Smallbone [a]

On 16th October 2017 ex-hurricane Ophelia passed over the UK, bringing with it a unique mixture of particulates which caused the sky to turn a dramatic red colour. Here we use an ensemble of modelling and remote sensing techniques in a 'top-down, bottom-up' approach comprising instruments onboard orbital platforms and a ground-based lidar, to interrogate the particle loading to determine its composition and origins. Using a novel, miniature lidar system and back-trajectory modelling to link the measurements to sources, we show that the event comprised two distinct phases, the first dominated by Saharan dust (volume depolarisation ratio at 532 nm; $\delta = 0.15–0.25$) and the second by an optically dense layer, starting at ~0.7 km, comprising a mixture of Saharan dust and biomass burning particles ($\delta = 0.08–0.18$) originating from intense wildfires in the Iberian Peninsula. CO levels in the weather system were measured as high as ~273 ppbV and the aerosol index to be >5. Also, the Ophelia system was probed for the first time using multi-spectral imaging data from the Multispectral Instrument (MSI) onboard Sentinel-2. This allowed the differentiation of cloud composition types from above by virtue of the different spectral signatures of the components of the cloud matrix and in doing so gave important supporting evidence to complement the ground-based lidar observations.

Environmental significance

Throughout the day of 16th October 2017, a dramatic, entirely unique atmospheric event occurred over the UK. As ex-hurricane Ophelia brought complex mixed aerosol layers north, skies turned an eerie orangey-red. Our paper adds to the very small body of work reporting on this unique event; it brings new analyses (including multispectral cloud-top imaging) and expands the geographical and temporal coverage of the phenomenon. We demonstrate how a mixed method 'top-down, bottom-up' approach can be used to speciate components of a complex aerosol–cloud matrix and identify sources. This work is of environmental significance in terms of adding to a limited body of evidence to help explain an exceptionally rare atmospheric event, and also to assist in understanding of medium-to-long-range aerosol transport.

1 Introduction

On 16th October 2017 a low-pressure system skirted the west coast of Ireland. While these systems are fairly typical for this location and time of year, this particular system was of hurricane classification (designated 'Ophelia') just off the coast of the Iberian Peninsula. As Ophelia made its rapid approach towards Ireland it underwent an extratropical transition and its hurricane status was downgraded. But the winds associated with the now 'ex-hurricane Ophelia' were still of sufficient magnitude to be damaging for parts of Ireland. Strong winds were also experienced over Great Britain, but also, the sky and Sun during the day unexpectedly took on a dramatic reddish hue.

From space, outside of the Earth's atmosphere, the Sun appears as white owing to its emissions profile in the visible region of the electromagnetic spectrum. However, on Earth the human visual system (HVS) registers the Sun as being yellow; this is a result of (mainly) Rayleigh scattering by the molecules that comprise the Earth's atmospheric envelope.[1] Essentially, the constituent molecules (and the smallest fractions of suspended particles) of the atmosphere scatter (in an omnidirectional manner) the shorter wavelengths of incoming solar radiation more efficiently than the longer wavelengths.[1–3] As such, atmospheric Rayleigh scattering results in a greater amount of scattering of shorter wavelength violet, indigo and blue light, and in combination with enhanced sensitivity of the HVS to the blue wavelengths, this causes the sky to appear blue.[4] It follows that removal of blue wavelengths from incoming solar radiation results in the Sun appearing yellow to the HVS. When

---

[a] *Centre for Earth Observation Science, School of Environment and Technology, University of Brighton, Brighton, BN2 4GJ, UK. E-mail: k.p.wyche@brighton.ac.uk*

[b] *Department of Earth and Environment Sciences, University of Manchester, Manchester, M13 9PL, UK*

[c] *National Centre for Atmospheric Science, University of Manchester, Manchester, M13 9PL, UK*

the Sun is lower in the sky (*i.e.* at sunrise and sunset), sunlight has to traverse a longer path-length through the atmosphere, and moreover through the densest region of the lower atmosphere where air molecules and larger particles are abundant. Owing to increased Rayleigh scattering over this longer path-length and with the addition of Mie scattering by particulate matter, more of the shorter – medium (~green) wavelengths are removed from the incoming solar radiation, and the Sun and sky take on a more orange or red appearance.[1–3]

So, the question arises, what caused the Sun and sky over the UK to turn red in the middle of the day on 16th October 2017 when the Sun was high in the sky? The answer is atmospheric aerosol.[5–7] Aerosol is a collective term for solid or liquid particles or droplets that are suspended in the air.[8] While the lower portions of the atmosphere (primarily the troposphere and to some extent, the stratosphere) typically host a range of concentrations, sizes and species of aerosol particles, their abundance is usually too low to have a noticeable effect on sunlight during the day. However, in locations, or under particular scenarios (*e.g.* after volcanic eruptions[9]), where the concentrations of ambient aerosol are high, the colour of sunlight can be reddened by scattering of the shorter – mid wavelengths by the aerosol. When the abundance of aerosol is very high, this scattering effect can make the Sun appear orangey-red, as on 16th October 2017 over the UK, where so much light was scattered that it was even possible to look directly at the Sun without causing damage to the eye. The amount of scattering that took place also led wide swathes of the UK sky to take on an unearthly orangey-yellow tint.

The aerosol scattering effect over the UK on 16th October 2017 was particularly dramatic because of a unique coincidence of several different factors. An initial topical report by Moore[6] (published in print in 2019) released shortly after the event indicated that the aerosol responsible for causing the '*red sky*' effect was likely to have comprised a mix of Saharan dust and forest fire particles transported from Africa and Portugal, respectively, by ex-hurricane Ophelia. Subsequent work by Harrison *et al.*[5] expanded on that of Moore[6] by reporting on detection of the aerosol within the Ophelia system using a radiosonde adapted to measure the electric charge of the atmosphere. These initial studies were followed by Osborne *et al.*,[7] who used the Met Office's Volcanic Ash monitoring network of ceilometers and lidar systems to provide a more detailed analysis of the layers of aerosol causing the scattering. Osborne and colleagues produced a time and height resolved map of the optically thick aerosol layers as they passed over the east of the UK, and using back trajectory modelling they showed that the air masses in question had previously traversed the Iberian Peninsula and the North Africa region.

Here we aim to bring new instruments and techniques to the study of this event and extend upon the work conducted by Osborne *et al.*[7] in analysing this phenomenon. Specifically, we add data from a new region and at a later time corresponding to the evolved weather system, which had begun to slow. In this work, we bring a new approach using a 'top-down, bottom-up' ensemble methodology, not only using space-based remote sensing data of atmospheric composition, but also for the first time, multispectral imaging of the cloud matrix within the weather system (employing the Multispectral Instrument (MSI), onboard Sentinel-2). In addition, from the ground-up, we use data from a new low-cost elastic backscatter Mini Micro Pulse lidar system (532 nm) to investigate the event in high temporal resolution, mapping the evolution of the cloud matrix composition and structure as the weather system made land-fall on the south coast of the UK.

Our mixed-method approach is employed here to successfully elucidate the composition and evolution of the aerosol–cloud matrix associated with ex-hurricane Ophelia, which caused the daytime sky to turn red during this relatively unstudied, completely unique event. In support of Osborne and colleagues, our findings indicate that the aerosol layer contained significant quantities of both desert dust and fire smoke. We also demonstrate how multispectral remote sensing imagery can be used to map the top of the aerosol cloud layer by virtue of the different spectral responses of the various aerosol populations present. Findings reported here will be of importance not only for those in the atmospheric and remote sensing measurement communities for the understanding of similar unique weather events, but also for modellers, to assist in their efforts to improve accuracies of medium to long-range aerosol transportation models.

2 Methodology

2.1 Satellite instruments

Multispectral remote sensing observations of the study area were acquired using five different instruments from one ESA and four NASA/NOAA operated satellite platforms. In order to visualise the cloud top (and extent) of Ophelia, corrected reflectance optical data were obtained from the MODerate resolution Imaging Spectroradiometer[10] (MODIS) (resolution, 250/500 m; imagery at 250 m) onboard NASA's EOS Terra platform (equatorial crossing time, 10:30) and from the Visible Infrared Imaging Radiometer Suite[11] (VIIRS) (resolution, 375/750 m; imagery at 250 m) onboard the NASA/NOAA Suomi NPP platform (equatorial crossing time, 13:30). VIIRS was also employed to provide Aerosol Optical Thickness (AOT) data to help identify the Saharan dust haze, and to identify locations of forest fires as thermal anomalies. VIIRS (Deep Blue) AOT data (resolution, 6 km at nadir; imagery at 2 km at nadir) were derived from the AERDB_L2_VIIRS_SNPP data product,[12] and the thermal anomaly data were obtained from the (day and night) VNP14IMG_NRT, Active Fire product.[13]

In order to track emissions from the Portuguese wild fires, the concentrations of carbon monoxide (CO) at 500 hPa (altitude, ~5.5 km) were obtained from the Atmospheric InfraRed Sounder[14] (AIRS) carried on NASA's EOS Aqua satellite (equatorial crossing time, 13:45). In this instance, the AIRS CO L3 data product was used, providing CO concentrations in mixing ratio units (ppbV) on a $1^\circ \times 1^\circ$ grid. Dust and biomass burning aerosol within the cloud matrix of ex-hurricane Ophelia were investigated using the Aerosol Index (AI) product[15] generated from data recorded by the Ozone Monitoring Instrument[16] (OMI) onboard NASA's EOS Aura satellite (equatorial crossing

Table 1 Sentinel-2 MSI band combinations employed[a]

Band combination	Spectral region	Band central wavelength/μm	Purpose
4, 3, 2	Red, green, blue	0.665, 0.560, 0.490	Visualisation of the scene
12, 11, 8A	SWIR, SWIR, VRE	2.190, 1.610, 0.865	Separation of cloud types
1, 4, 12	Coastal aerosol, red, SWIR	0.443, 0.665, 2.190	Separation of clouds from aerosol
12, 8, 4	SWIR, NIR, red	2.190, 0.842, 0.665	Separation of clouds from aerosol

[a] Notes: SWIR = short-wave infrared; VRE = vegetation red edge; NIR = Near infrared.

time, 13:45). OMI's Aerosol Index product (resolution, 25 km) is a qualitative parameter derived from L2 near UV Aerosol Optical Depth and Single Scattering Albedo data (OMAERUV), which can be used to detect the presence of atmospheric aerosol even "through mixed cloudy scenes".[17,18] MODIS, VIIRS, AIRS and OMI data were obtained from, and visualised using, NASA's Earth Observing System Data and Information System (EOSDIS) Worldview on-line tool (https://worldview.earthdata.nasa.gov/).

While MODIS-Terra and VIIRS Suomi NPP data were used to provide imagery of the entire weather system over a wide swath width (*i.e.* 2330 and 3060 km, respectively), higher resolution (10–60 m) Multispectral Instrument[19] (MSI) Sentinel-2 (equatorial crossing time, 10:30) data were used to interrogate the composition of Ophelia's aerosol–cloud matrix as it passed over the south coast of the UK and the ground-based lidar system. The Level 1C top-of-atmosphere reflectance product was used in this instance, so as to avoid the unwanted removal of important atmospheric data. The MSI Sentinel-2 data were obtained from ESA's Copernicus Open Access Hub (https://scihub.copernicus.eu/) and processed and visualised using the Sentinel Application Platform (SNAP). Here, the MSI measured reflectances were used in a qualitative manner to visualise different components of the Ophelia aerosol–cloud matrix by virtue of their different reflectance properties across the wavelength range.[20] More specifically, to interrogate the composition of the atmosphere during the *red sky* event four different band combinations were employed to make four different, yet complementary, composite images (one true colour and three false colour), where the different reflective properties of the water cloud, ice and various types of aerosol particles in the scene result in their representations presenting as different colour combinations. The band combinations employed were chosen according to current understanding of spectral response profiles and known absorption features for water cloud, ice cloud and aerosol particles, following (for example) work by Gao *et al.*,[21] Stammes *et al.*,[22] Qu *et al.*,[23] Park *et al.*,[24] and Gautam *et al.*;[20] details are given in Table 1.

A summary of all platforms, instruments and products used in this study, and information on image processing heritage are given in Table 2.

2.2 Lidar measurements

Ground-based lidar measurements were made from the south coast of the UK in the city of Brighton and Hove (50.86 N, 0.09 W) using a MiniMPL-532-C elastic backscatter Mini Micro Pulse Lidar (MiniMPL) system (Droplet Measurement Technologies, US). The MiniMPL comprises a 532 nm Nd:YAG laser, photon collection and measurement system and computer electronics. The MiniMPL has a programmable vertical resolution of 5–75 m and a maximum range of 30 km under clear sky conditions (as with all lidar systems, effective range of the MiniMPL is limited by the presence and density of cloud and aerosol). For this study, MiniMPL data were acquired with a vertical resolution of 30 m and a time resolution of 5 minutes. For further details of the MiniMPL system see for example, Spinhirne,[25] Eck *et al.*,[26] and Höpner *et al.*[27]

A lidar operates by emitting pulses of light vertically (for the purpose of this study) into the atmosphere, where they are scattered by molecules or aerosol (particles). The scattered light pulses are reflected back down to the instrument where they are collected and analysed.[25] Depending on a lidar's sophistication, various atmospheric parameters can be determined from interrogation of the returned pulses. With a basic lidar system, the time a pulse takes to travel to the target and back, and the intensity of the reflected light can be used to infer cloud base or

Table 2 Summary of orbital platforms, instruments and products used, and imagery derivation

Platform	Instrument	Equatorial crossing time	Application	Product	Processed and visualised by
NASA EOS Terra	MODIS	10:30	Optical imagery	Corrected reflectance true colour (1, 4, 3) derived from the MODIS level 1B product	NASA Worldview
NASA/NOAA Suomi NPP	VIIRS	13:30	Optical imagery	Corrected reflectance true colour (I1, M4, M3)	NASA Worldview
			Aerosol optical thickness	AERDB_L2_VIIRS_SNPP	NASA Worldview
			Active fires	VNP14IMG_NRT	NASA Worldview
NASA EOS Aqua	AIRS	13:30	CO	AIRS CO L3	NASA Worldview
NASA EOS Aura	OMI	13:45	Aerosol index	OMAERUV	NASA Worldview
ESA Sentinel-2	MSI	10:30	Optical imagery	Level 1C top-of-atmosphere reflectance	Authors

the location of an aerosol layer. Further, the signal power of a lidar system, which is proportional to the amount of laser light returned from the atmosphere, can be used to infer how much scattering is taking place in the atmosphere by both air molecules and aerosol particles.[25,28]

A standard lidar system has one receiver that measures the amount of light scattered back from the atmosphere irrespective of its polarisation. The MiniMPL employed here is a depolarisation lidar; it uses one receiver to measure the amount of backscattered light received both parallel and perpendicular compared to the transmitted laser light. It achieves this by alternately switching polarisation using a liquid crystal wave plate. Compared to lidars with two separate receivers, those with one combined receiver benefit from simplified calibration. From these two datasets aquired it is possible to see the extent to which the aerosol particles in the atmosphere have changed the polarisation of (or depolarised) the light since it was emitted. The volume depolarisation ratio[29] (δ_v or VDR) is defined in eqn (1), where $P_\parallel$ is the parallel signal power and $P_\perp$ is the perpendicular signal power. δ_v therefore represents the ratio of the perpendicular signal to the parallel signal and shows how much the scattering particles have depolarised the laser light. Spherical particles, such as liquid water cloud droplets or spherical aerosol particles, have a small depolarising effect and so their depolarisation ratio will be small. Conversely, non-spherical particles such as dust, ash and ice will have a large depolarising effect, so their VDR signal will be larger.

$$\delta_v = \frac{P_\perp}{P_\parallel} \tag{1}$$

While the VDR value is useful for identifying non-spherical particles, it is strongly dependent on particle type and concentration. Particle depolarisation ratio (δ_p or PDR) is commonly used to remove the effect of concentration and can aid in further identification of particle type. To obtain the PDR, the lidar backscatter profile is processed further to separate the effect of air molecules from the aerosol particles, resulting in the backscatter ratio ($\boldsymbol{R}$); this indicates how much of the lidar backscatter signal is due to aerosol. Ideally, this analysis is carried out using a multiple wavelength Raman lidar, as this type of system provides a reference backscatter profile at a different wavelength to separate the backscatter caused by the aerosol.[30] However, it is also possible to retrieve $\boldsymbol{R}$ with a single wavelength system by using a widely used aerosol inversion algorithm (*e.g.* Klett, 1981; Fernald *et al.*, 1984).[31,32] This algorithm relies on knowledge of the so-called Lidar Ratio (LR), which is defined by the ratio of aerosol extinction to aerosol backscatter. As the LR is different for different aerosol particle types and composition, this value assumes some prior knowledge of the particle type; as such for this study, values were employed from the literature. Using eqn (2) it is then possible to calculate the PDR:[33]

$$\delta_p = \frac{(1+\delta_m)\delta_v \boldsymbol{R} - (1+\delta_v)\delta_m}{(1+\delta_m)\boldsymbol{R} - (1+\delta_v)} \tag{2}$$

where δ_m is the depolarisation ratio of air molecules, which can be calculated based on knowledge of the lidar optics.[34] Relevant values can be found in Solanki *et al.*[35]

3 Results and discussion

3.1 Synoptic overview

On 15th October 2017, hurricane Ophelia was quickly moving north-eastwards towards the British Isles with a high-pressure system over central Europe. A strong north-easterly jet stream

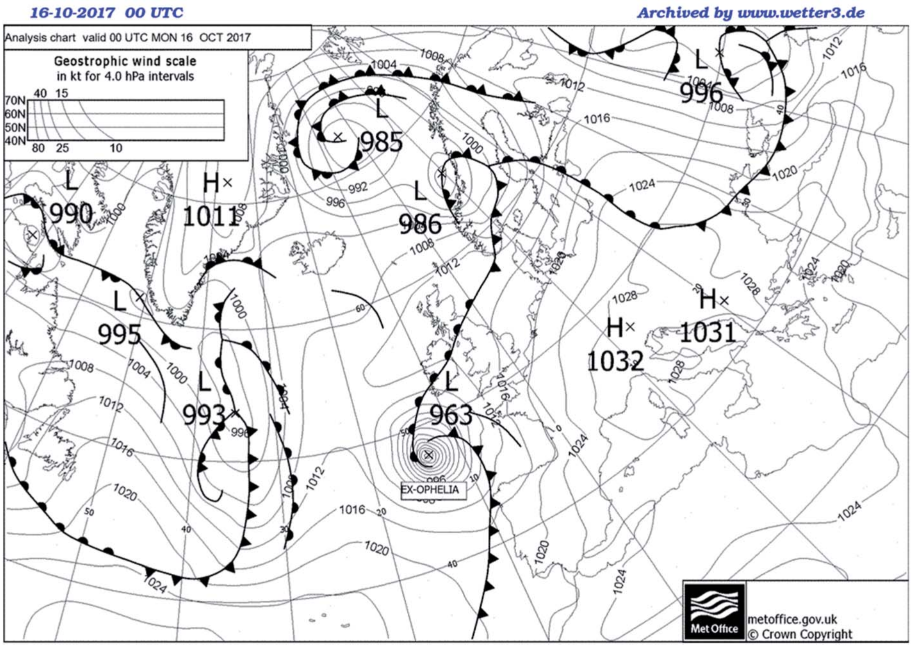

Fig. 1 Synoptic chart for 16th October 2017 at 00:00 UTC. 'Ex-Ophelia' denotes the newly transitioned extra-tropical cyclone (metoffice.gov.uk).

was in place between Scotland and Iceland. By 00:00 UTC on 16th October, Ophelia was undergoing its extra-tropical transition south-west of Ireland (Fig. 1). Having lost its hurricane status, Ophelia made landfall along the Irish coast on the morning of the 16th October 2017, with gusts reaching 155.6 km h^{-1} and record breaking 10-minutes average wind speeds for October in Ireland of 114.8 km h^{-1}.[36] Further east, the British coast also experienced strong, warm winds within the warm sector of the newly transitioned extra-tropical cyclone. These warm winds formed the warm conveyor belt (WCB) that flowed parallel to, and in front of the cold front, before being lifted over the warm front.

Fig. 2 shows the composite true colour RGB image of ex-hurricane Ophelia recorded by VIIRS onboard the NASA/NOAA Suomi NPP satellite, *ca.* 12:35–12:45 UTC (right-hand swath in the image) on 16th October 2017. This true colour VIIRS image clearly shows the extent of Ophelia, at this point designated an extra-tropical cyclone, and the associated cloud top over Ireland, the UK and Western Europe. The WCB can be identified by a narrow swath of cloud stretching from Portugal, over north-western France, up to southern England. Predominantly, the air in a WCB is warm and moist and therefore characterised by cloudy conditions, but in this case, warm and dry air was being transported up from lower latitudes leading to intermittently cloudy skies. Unusually in this instance, the WCB also contained enough aerosol to cause the skies over the UK to take on the observed dramatic reddish hue.

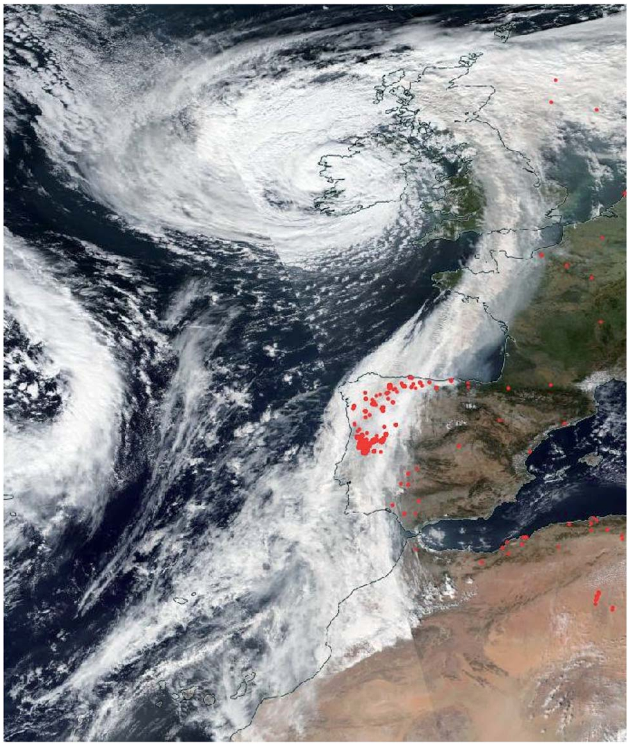

Fig. 2 True colour RGB corrected reflectance visualisation of the cloud top on 16th October 2017, derived from Suomi NPP VIIRS data. Areas of high-density heat anomalies, indicating fires, are highlighted as red dots (NASA Worldview).

3.2 Back trajectory analyses

In order to explain the dramatic reddening of the UK sky on the 16th October, the composition of the aerosol–cloud matrix that covered the region must be investigated further. The first stage in such an investigation is to determine the origins and transit paths of the air masses in which the aerosol was suspended. To do this, air parcel back trajectory simulations were conducted using the HYSPLIT transport and dispersion model provided by the NOAA Air Resources Laboratory (ARL);[37] the results are presented in Fig. 3.

Fig. 3 shows the HYSPLIT calculated back trajectories of the air parcels that arrived at a height of 2 km over Brighton between 02:00 and 23:00 UTC on 16th October 2017. New trajectories were started every 3 hours and were backcast for a period of 72 hours. The model showed that during the morning of the 16th, between 02:00 (blue) and 08:00 (yellow) UTC, air parcels arriving over Brighton had their origins off the north-west African and Iberian coasts at heights of ~1.0–2.4 km. The calculations showed that as the day progressed, between 11:00 (purple) and 17:00 (black) UTC, *i.e.* roughly around and after the time of acquisition of the VIIRS data shown in Fig. 2, the air shed was being brought directly from Portugal and northern Spain, and at times, from near ground level (*e.g.* 11:00, purple, on 14th and 15th October). The Iberian Peninsula and north-west Africa are both known to be significant source regions of atmospheric aerosol, from biomass burning smoke and the uplift of Saharan desert dust, respectively.[38,39] It was during this middle part of the day that the *red sky* phenomenon was observed. Later into the evening of the 16th October, *i.e.* 20:00 (pink) and 23:00 (orange), the HYSPLIT calculations showed that the direction from which air parcels were being imported had changed again, now their origins were the remote northern areas of the Atlantic Ocean towards Greenland, regions often associated with relatively cleaner air and lower aerosol loading,[40] and at much higher altitudes (*i.e.* >6.0 km).

3.3 Top-down: detailed satellite observations

On the 14th and 15th October, two days prior to the UK *red sky* event, a number of intense wildfires broke out in northern Portugal and across parts of north-west Spain.[6] These fires were still visible in the VIIRS Active Fire product on the 16th October and can be seen depicted as red dots in Fig. 2. Such large-scale biomass burning events are known to produce pyrocumulus plumes that contain significant quantities of aerosol and carbon monoxide gas,[41–46] and their presence has previously been linked to a reddening in the appearance of the sky in various geographical locations.[47–50]

The VIIRS optical imagery shown in Fig. 2 and the back-trajectory analysis presented in Fig. 3 indicate that the air shed over the UK on the 16th October 2017 can be traced yet further back, past Portugal and Spain towards north-west Africa and the Sahara region. With appropriate meteorological conditions, significant quantities of Saharan mineral dust can be uplifted into the atmosphere from the desert floor where it can remain suspended for days, reaching locations as far as South America and Scandinavia.[51] Such Saharan dust/haze

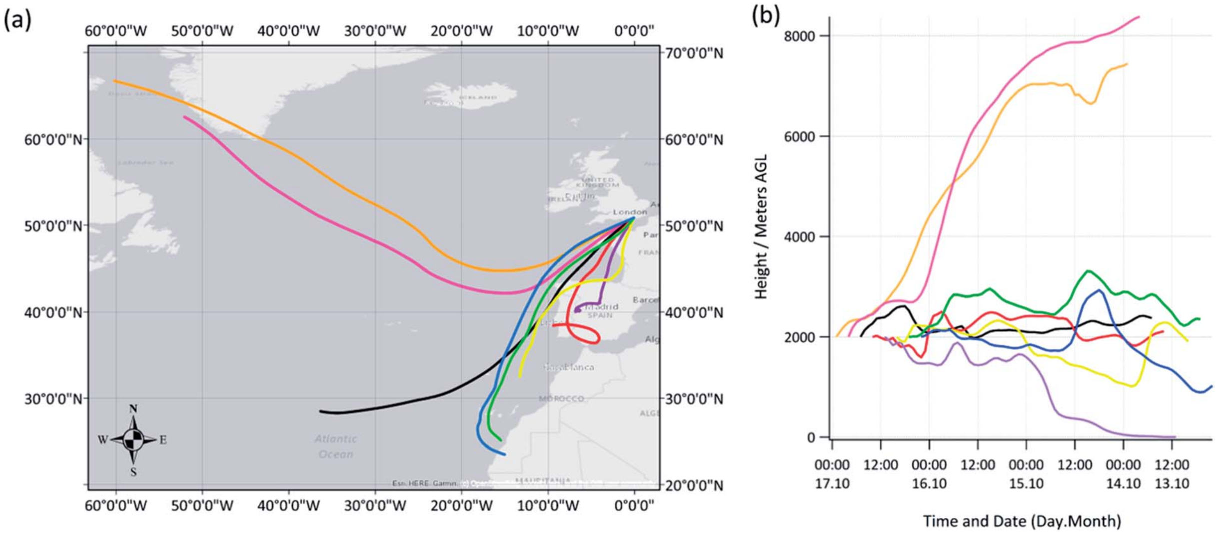

Fig. 3 (a) 72-hour HYSPLIT back trajectory analysis for air masses arriving over Brighton and Hove (50.86 N, 0.09 W) on 16th October 2017. New trajectories started every 3 hours at a height of 2000 m. 23:00 = orange, 20:00 = pink, 17:00 = black, 14:00 = red, 11:00 = purple, 08:00 = yellow, 05:00 = green, 02:00 = blue. (b) Trajectory heights. All times UTC.

events are known to influence European air quality, occasionally causing PM levels to reach, or rise above legislated air pollution limits.[52–54] As was noted by Osborne *et al.*[7] and Moore,[6] several days prior to the UK *red sky* event, large patches of Saharan dust haze were detected by various orbital remote sensing instruments, lying over the north-west of Africa and spreading out across the coast to the Atlantic Ocean. This haze can be clearly seen in the true colour RGB corrected reflectance VIIRS imagery in Fig. 4a, recorded on the 14th October 2017, just off the north-west African coast and to the south-east of hurricane Ophelia. Fig. 4b shows the concomitant Aerosol Optical Thickness (AOT) measurements also made by VIIRS, which reached particularly high levels of >1.5 at this time, indicating a dense, aerosol heavy haze layer with low light transmission.[55–57] It is worth noting here that recent studies have reported possible issues in the AOD product derived from VIIRS owing to the potential need for a fuller treatment of land surface (reflectance) and aerosol (property) types during retrieval.[58]

By comparing the VIIRS and MODIS (not shown) optical imagery, AOT data, Active Fires product and the HYSPLIT back-trajectory calculations with AIRS carbon monoxide (CO) and OMI Aerosol Index (AI) data, it is possible to see that the aerosol and CO produced by the Iberian biomass burning episodes of the 14–16th October 2017, and dust particles within the haze cloud uplifted from the Sahara region of North Africa, were incorporated into Ophelia's aerosol–cloud matrix and transported to the UK. This is shown in Fig. 5a, which gives the CO

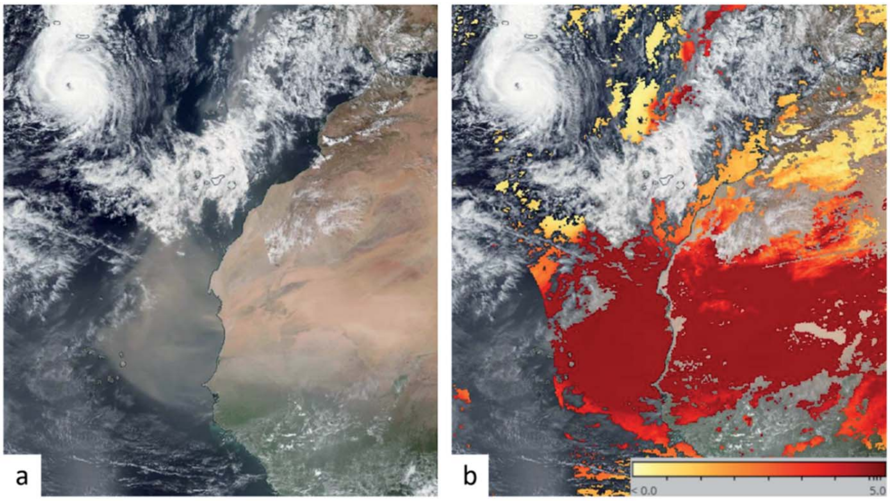

Fig. 4 (a) True colour RGB corrected reflectance visualisation of the mineral dust haze off the coast of north Africa on 14th October 2017 and (b) corresponding Aerosol Optical Thickness (AOT) obtained from Suomi NPP VIIRS (NASA Worldview).

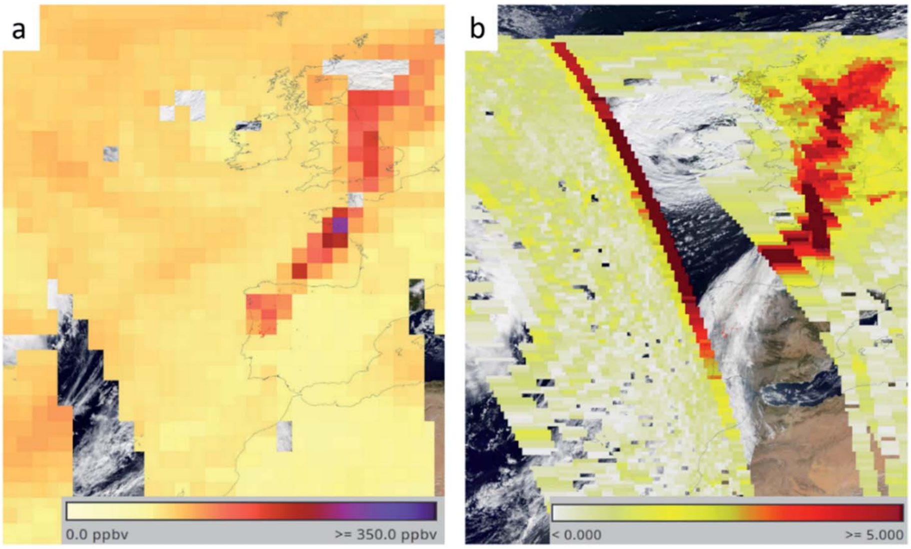

Fig. 5 (a) Carbon monoxide mixing ratio at 500 hPa on 16th October 2017 obtained from AIRS (Aqua), and (b) aerosol index on 16th October 2017 derived from OMI (Aura) data (both overlaid on MODIS true colour RGB imagery; NASA Worldview).

mixing ratio at 500 hPa recorded by AIRS between roughly 12:05 and 12:10 UTC (far right-hand swath in the image) and 13:40 and 13:48 UTC (central swath in the image), and in Fig. 5b, which gives the atmospheric AI measured by OMI between roughly 12:10 and 12:17 UTC (right-hand swath in the image) on the 16th October. As can be seen in Fig. 5a and b, CO and AI levels, respectively, were very high in a distinct band aligning with Ophelia's cloud-top, stretching from Portugal to much of the UK. The CO mixing ratio of the aerosol–cloud matrix was recorded as being as high as 273 ppbV and the AI value >5, indicating a linkage to fire sources and a significant loading of desert dust and soot-like particles.[59–64]

Sentinel-2 MSI data recorded on the day of the *red sky* event is shown in Fig. 6 and Table 3 provides a qualitative description of the key atmospheric features apparent in each of the images. The data are displayed at 60 m resolution and represent a composite of multiple scenes acquired in a continuous manner. The data have not been atmospherically corrected so as to avoid the unwanted removal of important atmospheric information.

Fig. 6a gives the true colour representation of the scene, with the west coast of France evident along the left edge of the image and the south coast of the UK located at the top. The location of the *in situ* equipment for lidar data acquisition is represented by a red cross. As with the VIIRS imagery, the water and ice cloud within the Ophelia system can be clearly identified as a white/wispy white band (*cf.* Table 3) running from top to bottom along the image.

The false colour composite using Sentinel-2 MSI bands 12, 11, 8A is shown in Fig. 6b. This composite allows distinct separation of cloud types through the significant differences evident between the reflectance spectra of water cloud and ice cloud in the lower end of the Short-Wave Infrared (SWIR; band 11, 1.6 μm) and the Vegetation Red Edge (VRE; band 8A, 0.865 μm) regions.[21,22,24] More specifically, both cloud types have similarly strong reflectance responses in the red edge region, yet around 1.6 μm in the SWIR, ice cloud has relatively weaker reflectance. The distinct difference in reflectance between water clouds and ice clouds in this SWIR region is evidenced in work by Gao *et al.*[21] and Qu *et al.*,[23] with spectral profiles indicating that this wavelength represents a local peak in the water cloud reflectance response and a corresponding enhanced absorption for ice cloud. When purple is shown in Fig. 6b this represents a relatively similar and elevated level of reflectance recorded in both the SWIR region of band 12 (*i.e.* 2.19 μm) and the Vegetation Red Edge region, but lower reflectance in the SWIR1 band 11 owing to low moisture content, indicating the dry nature of the air mass. This is in-line with data presented by Harrison *et al.*,[5] which indicated that regions of this air mass were "anomalously dry" (pp. 8). The low-level contribution of band 11 (1.6 μm), which allows the purple colour (*cf.* Table 3), indicates that the features comprise ice cloud.[21–24] Water cloud is relatively more reflective in band 11 and absorbs in the VRE region, relative to the consistent nature of ice cloud, to give an orange appearance in the image (*cf.* Table 3). The low reflectance of aerosol (consisting of smoke and dust) ensures that it is not as visually prominent in this particular composite, which makes for an interesting and stark contrast with the other images presented in Fig. 6.

To identify the location of the aerosol particles, the band combinations of band 1 (coastal aerosol, 0.443 μm), band 4 (red, 0.665 μm) and band 12 were used in Fig. 6c to capitalise on differences existing with the water and ice cloud types. Using this combination, the clouds can be separated from the aerosol, with the aerosol absorbing the band 12 SWIR radiation to a greater extent than the cloud mixtures, particularly the water clouds, which as a result are much more separable.[20,23] The burnt yellow appearance of the aerosol is achieved through a slight relative reduction in reflectance of band 4, which

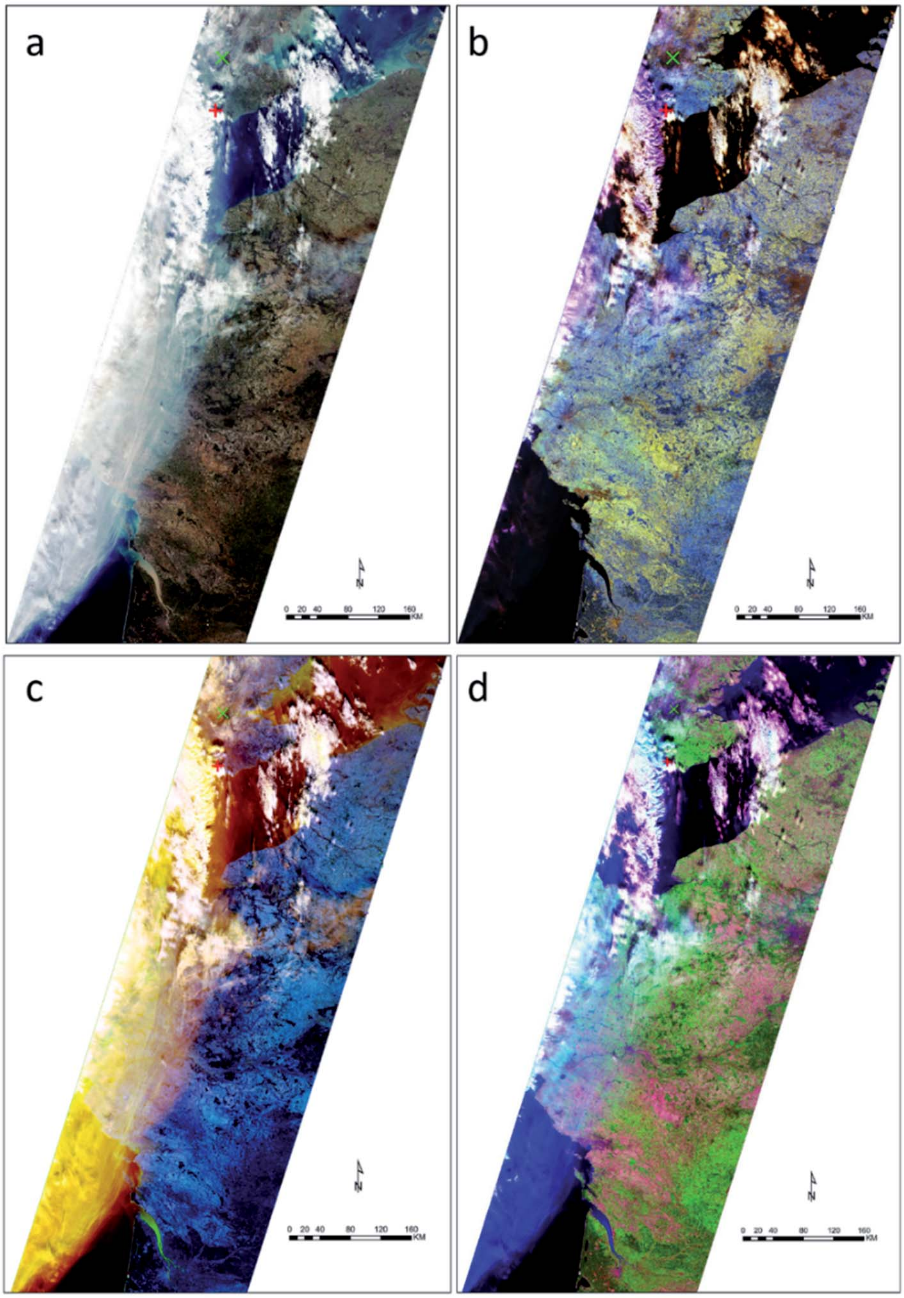

Fig. 6 Full swath Sentinel-2 imagery of the cloud top of the ex-hurricane Ophelia aerosol–cloud matrix over parts of France and the UK on the 16th October 2017. (a) True colour RGB image using band combination 4, 3, 2; (b) false colour RGB image using band combination 12, 11, 8A; (c) false colour RGB image using band combination 1, 4, 12; (d) false colour RGB image using band combination 12, 8, 4. See text for details.

represents red light (*cf.* Table 3). This light is absorbed and internally scattered within the aerosol media.

Fig. 6d reinforces the interpretation of Fig. 6c, with the royal blue hue in the image a result of absorption by aerosol in band 12 and band 8 (near infrared, 0.842 μm) (*cf.* Table 3), combined with relatively strong reflectance in band 4 with respect to the levels exhibited by clear sky over the Atlantic Ocean. The water cloud in this image is represented strongly by the purple colour, with the ice cloud showing more similarities in reflectance to the aerosol than is the case for the water cloud owing to the respective low reflectance in the featured SWIR region (2.19 μm).

Fig. 7 focuses more closely (∼11:00 UTC) on the region around Brighton and Hove (red cross). In Fig. 7 it is possible to define the three different types of cloud discussed above plus areas of mixing between the different types. As described earlier, the water clouds can be easily distinguished to the east and west of the image but embedded in these in the west appear to be ice cloud and aerosol. The aerosol signature is more apparent to the north of Brighton surrounding London (green

Table 3 Sentinel-2 band combination image appearance description

Image description				
Channels	4, 3, 2	12, 11, 8A	1, 4, 12	12, 8, 4
Figure	Fig. 6a	Fig. 6b	Fig. 6c	Fig. 6d
(1) Water cloud	White	White (orange edges)	White (with shadow)	White (purple edges)
(2) Ice cloud	Wispy white	Purple (white where thicker)	Yellow (white where thicker)	Cyan (white where thicker)
(3) Aerosol (smoke/dust)	Murky	Not visible (visible in low level purple/white hue)	Yellow orange	Faded royal blue (with blue/white hue)
(4) Mixed cloud and aerosol[a]	Combination of the above			

[a] Mixing complicates the image interpretation with spectral profiles of aerosol features combining in such a manner as to mask the otherwise distinctive spectral characteristics. This can in places equalise the reflectance across the bands to lead to greyscale features in the image, in this instance with mixed areas tending towards white appearance.

cross representing Greenwich Meridian) as seen in Fig. 7c and d where there is less cloud presence. The aforementioned mixing can be seen to the west and north of the image. The significant degree of cloud and aerosol mixing does complicate spectral thresholding throughout the region but nevertheless key distinctions are apparent and align with the lidar data, which can be used as a guide to optical thickness.

3.4 Bottom-up: detailed lidar observations

Remote sensing data recorded by instruments onboard space-based platforms in low Earth orbit provide extremely useful information over large areas of the globe, but owing to their orbital parameters, their revisit times are restricted to typically one sunlit overpass of a given location each day, hence their temporal resolution is relatively poor. As such, in this instance, VIIRS, MODIS, MSI, OMI and AIRS provided only a 'snapshot' of the Ophelia system as it passed over the UK. In order to make a more detailed investigation of phenomena such as the Ophelia aerosol–cloud matrix, higher time resolution, ground-based systems are required to provide complementary data to those supplied by instruments onboard orbital platforms. To bridge the data gap here, the vertically pointing, ground-based elastic backscatter Mini Micro Pulse Lidar system described in Section 2.2 was employed; Fig. 8 shows the data recorded. More specifically, Fig. 8a shows the total (combined co-polarised and cross-polarised) normalised relative backscatter signal received by the lidar; these data identify anything that is scattering light in the atmosphere, *e.g.* cloud droplets, aerosol, ice particles, *etc.* and Fig. 8b shows the volume depolarisation ratio (VDR) representing the ratio of the perpendicular lidar backscatter intensity to the parallel lidar backscatter intensity (see Methodology). Low VDR values indicate the presence of spherical particles in the target air matrix, such as pollution aerosol or water droplets and higher values indicate non-spherical particles such as dust, ash and ice crystals.

From detailed inspection of the MiniMPL data in Fig. 8, it is clear that the *red sky* event can be split into two distinct time phases, *i.e.* 00:00–10:00 UTC and 10:00–22:00 UTC, during which several specific features were evident in the data, these are marked as (i) to (viii) in Fig. 8 and are discussed in detail below.

3.4.1 Before 10:00 UTC. On 16th October 2017 between roughly 00:00 and 10:00 UTC the atmospheric measurements made above Brighton and Hove by the MiniMPL showed the presence of a deep layer of aerosol reaching up from the surface to roughly 5 km in height, this is labelled as region (i) in Fig. 8. The green colour in Fig. 8a indicates the presence of aerosol and the change in colour shows the layering of the different aerosol air masses. The relatively high VDR ratios of generally ∼15–25% (excluding outliers) between roughly 0.5 and 4 km, seen in Fig. 8b, suggest the presence of non-spherical aerosol in this region at this time.[39,65] Lidar volume depolarization ratios of this order have previously been found to be consistent with Saharan and other mineral dust aerosol.[33,39,65–68] Therefore, coupled with the HYSPLIT back trajectory analysis and ensemble satellite remote sensing observations, the MiniMPL data in region (i) can be interpreted as Saharan dust aerosol residing within the warm conveyor belt of ex-hurricane Ophelia as it passed over Brighton and Hove. The returned lidar signal power was roughly similar throughout region (i) (Fig. 8a), but below 0.5 km the VDR was somewhat lower, of the order 6–10% (Fig. 8b); this region is labelled as (ii) in Fig. 8, and is indicative of this segment of the air mass being made up of a mixture of dust and more typical anthropogenic aerosol which tends to be spherical and therefore has a lower depolarisation ratio.[67,69] Region (iii) in Fig. 8, between roughly 4 and 6 km, shows the base of a strongly absorbing cloud layer within the system (depicted in yellow in Fig. 8a). Here, the absorption was so strong in places that the lidar beam was unable to penetrate to higher altitudes (indicated by the dark blue and white colours in Fig. 8a above 4–8 km). The data as presented in Fig. 8b show that region (iii) comprised a distinct layer of low VDR (*i.e.* below 5%; seen as dark blue colours in Fig. 8b), below a thin layer of slightly higher VDR (*i.e.* in the general range 9–15%; seen as green colours in Fig. 8b), punctuated with transient sections of very high VDR values (*i.e.* above 30%; seen as yellow colours in Fig. 8b). The differences in VDR in this layer can be explained by the presence of water droplets (lower VDR values) and (solid) ice particles (higher VDR values); as reported earlier, both water

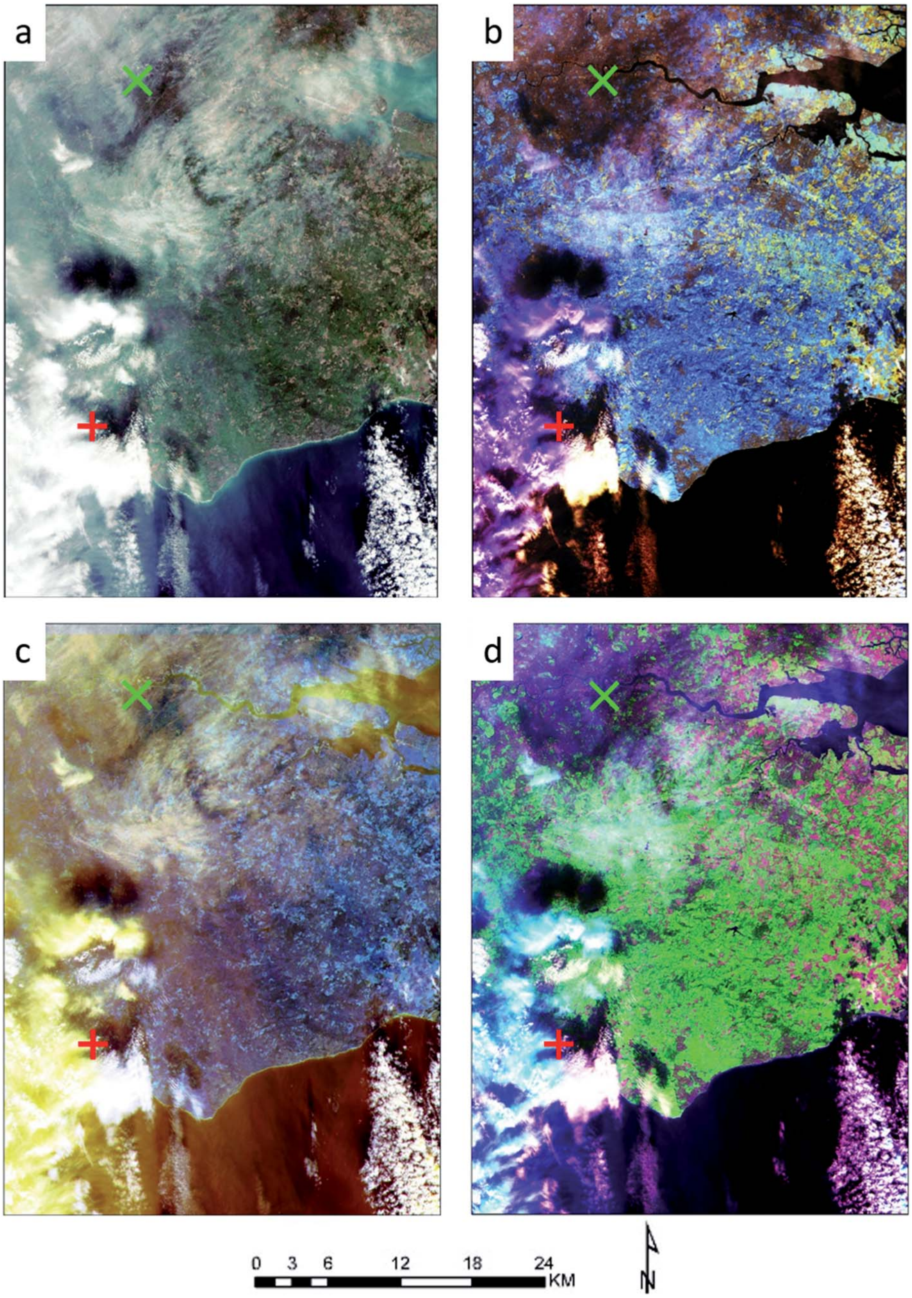

Fig. 7 Sentinel-2 imagery of the cloud tops over the south of the UK on the 16th October 2017. (a) True colour RGB image using band combination 4, 3, 2; (b) false colour RGB image using band combination 12, 11, 8A; (c) false colour RGB image using band combination 1, 4, 12; (d) false colour RGB image using band combination 12, 8, 4. See text for details.

and ice cloud features were detected in the Sentinel-2 MSI imagery. The short-lived vertical aerosol features evident in Fig. 8, for example (iv), indicate the occurrence of transient precipitation events. Unfortunately, owing to logistical issues it was not possible to fully calibrate the polarisation of the lidar during the study and as such there may be an offset in the VDR values reported here.

Further analysis to retrieve the PDR was only possible for a brief cloud free period shortly after 00:00 UTC (Fig. 9 and Table 4). Between 00:22 and 00:35 UTC a layer between 1.0 and 5.0 km showed a strong depolarisation signal, indicating the presence of non-spherical particles. The calculated PDR for this layer was between 0.27 and 0.42, with a median of 0.39. Again, it was not possible in this instance to fully calibrate the VDR values, which could have led to a bias in the PDR calculations. However, the range of values found here do broadly agree with PDR values observed for Saharan dust in other studies (although it is recognised that the median and upper limit reported here are higher).[68,70] A direct comparison with Osborne *et al.*[7] was not possible in this instance, owing to our

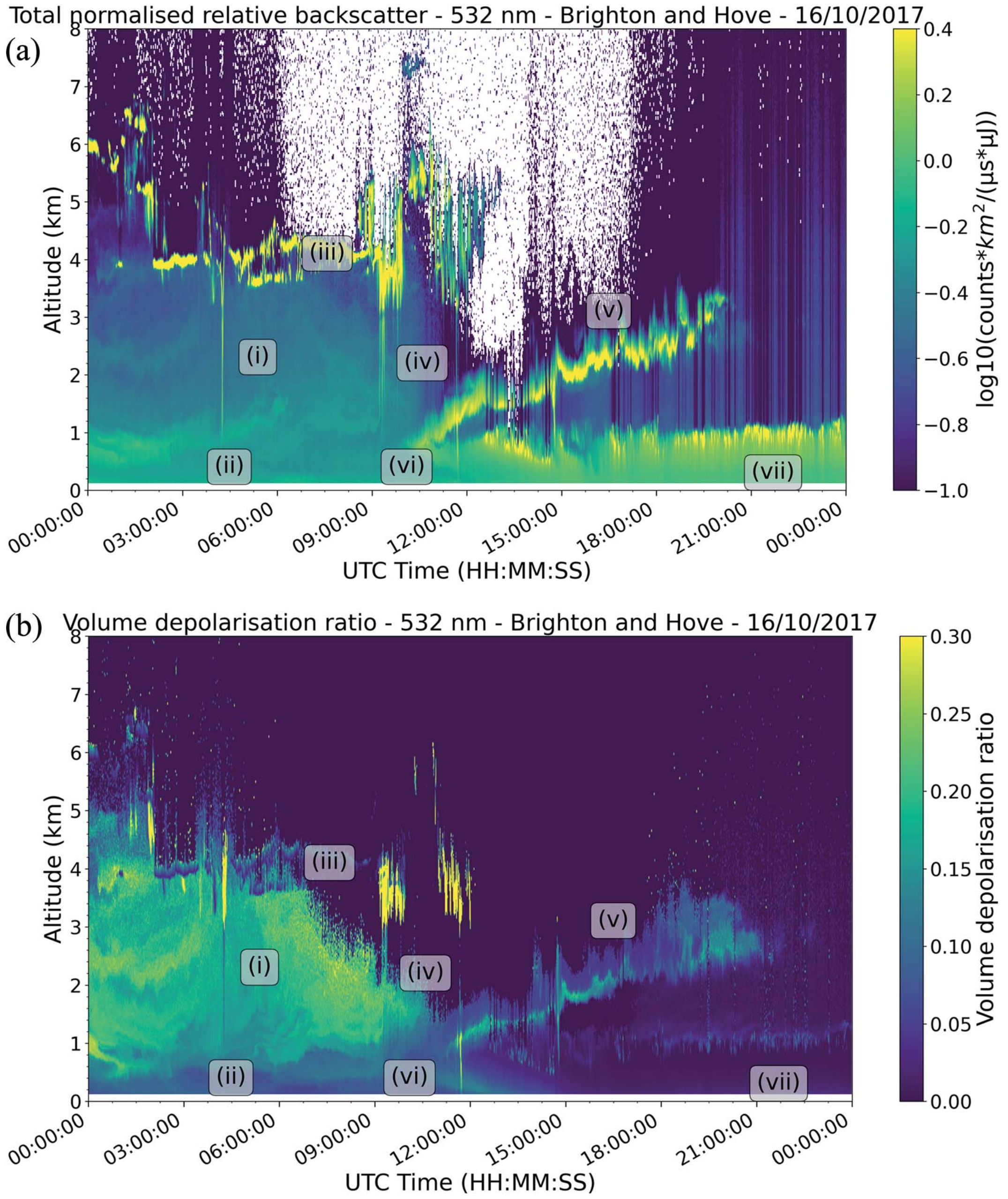

Fig. 8 Observations from the Mini Micro Pulse Lidar (MiniMPL) system in Brighton on the 16th October 2017. (a) Range corrected total (combined co-polarised and cross-polarised) normalised relative backscatter signal and (b) volume depolarisation ratio. (i) Saharan dust: very high depolarisation ratio, deep layer; (ii) spherical aerosol and dust mix; (iii) cloud base: strong extinction; (iv) rain shower: short duration vertical features, high backscatter, low depolarisation ratio; (v) smoke/dust layer: diffuse base unlike cloud base, high depolarisation ratio, laser penetrates later as optical thickness decreases; (vi) high depolarisation ratio as air is entrained from layer (v); (vii) non-smoke/non-dust layer: droplets, different wind direction, very low depolarisation ratio.

respective studies using lidars operating at different wavelengths.

In summary, the ensemble data show that during the time period 00:00–10:00 UTC, the warm, dry air mass over Brighton and Hove was dominated by the presence of Saharan dust that had been transported to the south of the UK within the warm sector of the recently transitioned Ophelia system.

3.4.2 After 10:00 UTC. Between roughly 10:00 and 21:00 UTC, the MiniMPL data shows that the Ophelia aerosol–cloud matrix was dominated by a strongly absorbing layer, labelled as region (v) in Fig. 8. The base of this layer appeared at ∼0.7 km at ∼10:00 UTC and rose to a height of roughly 2.4 km by ∼21:00 UTC, as shown in terms of backscatter signal in Fig. 8 and 10. Between roughly 10:00 and 12:00 UTC and after 18:00 UTC, the laser beam from the lidar was able to penetrate layer (v), as indicated by the observable cloud layer in the retrieval shown in Fig. 8 between 4 km and 6 km and the visible lidar return (in blue) above it. Between roughly 12:00 and 18:00 UTC the layer

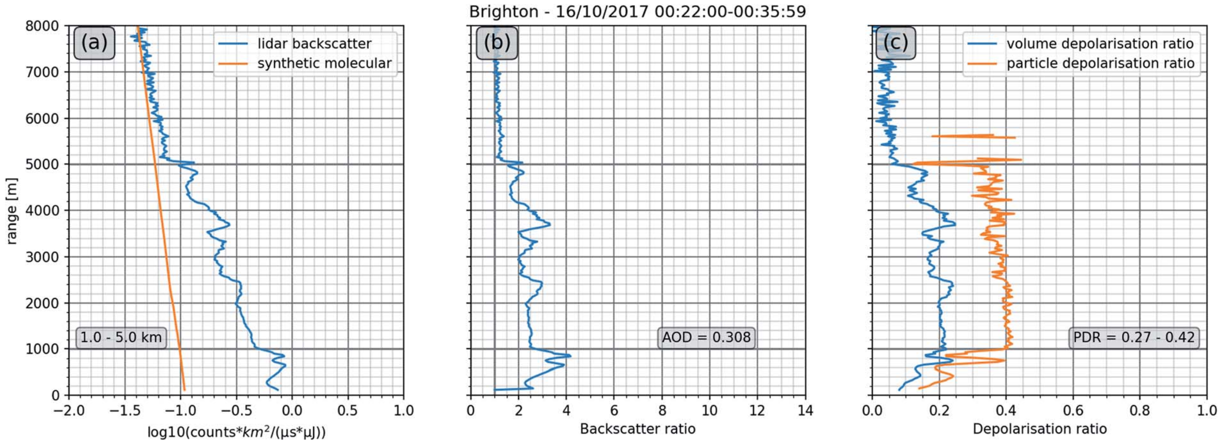

Fig. 9 Lidar data averaged for 16th October 2017 00:22:00–00:35:59 UTC: (a) total normalised relative backscatter signal as shown in Fig. 8 along with the 'synthetic molecular' backscatter (this is the backscatter derived from a nearby radiosonde that mimics an atmosphere that does not contain any aerosol). (b) Backscatter ratio calculated by application of a Klett retrieval algorithm as described in Section 2.2. The aerosol optical depth (AOD) shown is based on an assumed lidar ratio of 50 sr. (c) VDR and PDR (PDR masked where the backscatter ratio dropped below 1.25).

Table 4 Lidar retrievals from different layers as shown in Fig. 9 and 11

Time (UTC)	Layer altitude	AOD	PDR range	PDR median
00:22–00:35	1.0–5.0 km	0.31 ± 0.03	0.27–0.42	0.39
20:00–20:07	2.3–3.16 km	0.042 ± 0.010	0.19–0.36	0.28
20:00–20:07	3.16–3.5 km	0.10 ± 0.02	0.10–0.13	0.11
20:34–20:48	2.4–2.9 km	0.013 ± 0.002	0.35–0.46	0.39

was too optically thick for the laser to penetrate (as shown by white pixels in Fig. 8a), so the full depth of layer (v) at this time is not known.

Layer (v) presented similar to cloud layer (iii) which was observed earlier in the day, with a strong backscatter signal that decreased rapidly above the signal peak (Fig. 8a). However, unlike layer (iii), layer (v) did not appear to be dominated by water droplets, as indicated by the generally higher VDRs recorded by the MiniMPL, which were in the approximate range 8–18% (excluding outliers; Fig. 8b). The dominant scattering particles in this instance were also unlikely to have been ice particles as they were residing in a warmer air mass than those that were identified in layer (iii). The volume depolarisation values within layer (v) were higher than those of the cloud base of layer (iii) (excluding the transient sections where VDR was >30%, which presumably resulted from the presence of ice particles), but not as high as those recorded in region (i), which contained Saharan dust aerosol. Volume depolarisation ratios of the order 10–20% are indicative of layer (v) comprising a mixture of both spherical and non-spherical particles.[65] The decrease in VDR with height is most likely explained by the presence of particles with greater terminal velocity and higher VDR falling out of the layer. This was not likely to have been caused by multiple scattering, as additional scattering events would have depolarised the light further and increased the depolarisation ratio.[71,72]

Previous studies using 532 nm lidar systems have shown that lower volume depolarization ratios of the order <10% are consistent with the presence of spherical biomass burning/

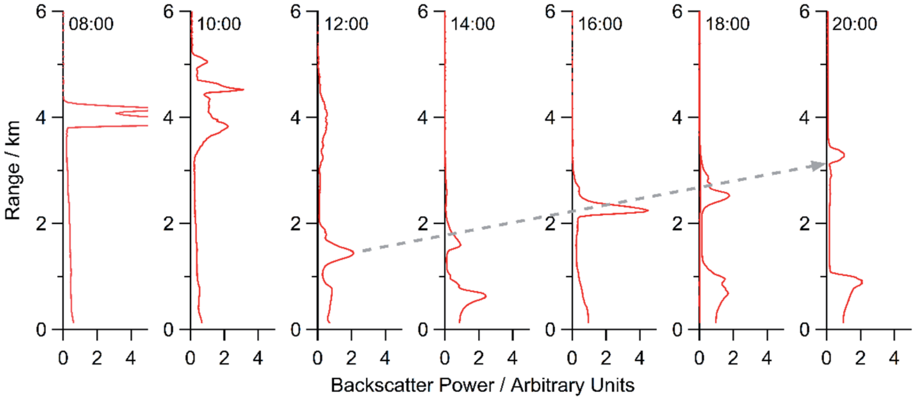

Fig. 10 MiniMPL range corrected co-polarisation normalised relative backscatter signal above Brighton and Hove on the 16th October 2017 at 2-hourly intervals between 08:00 and 20:00 UTC. The grey dashed arrow shows the base of the optically dense layer rising throughout the afternoon.

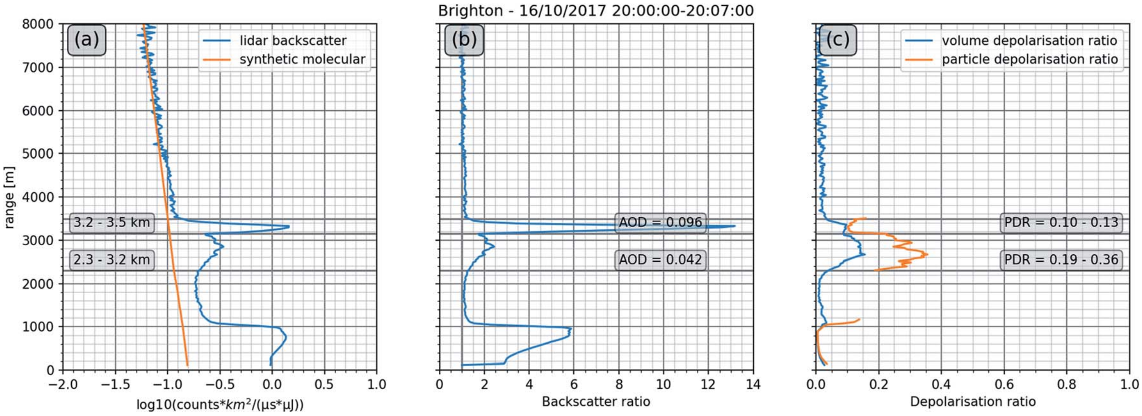

Fig. 11 Lidar data averaged for 16th October 2017 20:00:00–20:07:00 UTC: (a) total normalised relative backscatter signal as shown in Fig. 8 along with the 'synthetic molecular' backscatter (this is the backscatter derived from a nearby radiosonde that mimics an atmosphere that does not contain any aerosol). (b) Backscatter ratio calculated by application of a Klett retrieval algorithm as described in Section 2.2. The aerosol optical depth (AOD) shown is based on an assumed lidar ratio of 50 sr. (c) VDR and PDR (PDR masked where the backscatter ratio dropped below 1.25).

smoke particles,[67] and that intermediate volume depolarization ratios of ∼15% are consistent with an air mass containing a mixture of biomass burning particles and mineral dust.[65] Looking at the HYSPLIT back trajectories for the timeframe when the optically dense layer (region (v)) passed over Brighton and Hove (Fig. 3, 10:00–17:00 UTC), they show that the air parcels were originating from/passing over Portugal and northern Spain; the locations of the wildfires from the preceding days. Therefore collectively, findings from the MiniMPL, back trajectory analysis and satellite imagery indicate that the optically dense layer (region (v)) within the Ophelia aerosol–cloud matrix is likely to have contained biomass burning aerosol particles. As with region (i), the air mass of region (v) was still part of the warm sector of the Ophelia system and therefore would also have originated from the regions around northern Africa. As such, the optically dense layer most likely also included some Saharan dust (as indicated by the intermediate VDR values ∼10–20%), but was dominated by forest fire smoke. This finding is in-line with the conclusions of Osborne *et al.*[7] working on data recorded earlier in the day from measurement sites located in the west and north of the UK.

Initially during the post-10:00 UTC phase of the *red sky* event, *i.e.* between roughly 10:00 and 12:00 UTC, the aerosol from layer (v) was mixed into the atmospheric boundary layer (shown as high VDR values in region (vi) of Fig. 8). However, after 12:00 UTC the boundary layer and the dust/smoke layer became decoupled, and the boundary layer (labelled as (vii) in Fig. 8) went on to be dominated by spherical aerosol, as indicated by the low volume depolarisation ratios seen in Fig. 8b, which are typical of locally emitted pollution.[67,73,74] This decoupling was due to the change in wind direction with height; *i.e.* the air mass in and above layer (v) was at the time being governed by warm south-westerly winds within the warm sector, whereas the air below layer (v) was originating from the north west, being brought in from the North Atlantic.

This decoupling allowed retrieval of the extinction-to-backscatter ratio (or lidar ratio) using a retrieval method that requires a layer of aerosol-free air both above and below the target aerosol layer.[75] The lidar ratio provides an indication of the type of aerosol present.[69] After averaging the lidar data (20:05–20:35 UTC) the lidar ratio was found to be in the range of 40–60 sr. A direct comparison with Osborne *et al.*[7] was again not possible owing to the different wavelengths of the lidar systems employed in our respective studies. However, previous work has shown that biomass burning particles tend to have a slightly higher lidar ratio when measured by UV lidars compared to visible lidars;[69,76] taking this into account, our findings appear to be broadly in agreement with those of Osborne *et al.*[7]

Later in the day the aerosol-free air above the target aerosol layer allowed retrieval of the PDR. Between 20:00 and 20:07 UTC (Fig. 11 and Table 4) the aerosol could be separated into two distinct layers. The upper layer (3.16–3.5 km) presented as a strongly scattering aerosol laden area with an AOD of 0.100 (±0.020) and a PDR of 0.10–0.13; this identifies as biomass burning aerosol when compared with previous studies.[76] The lower layer, directly below (2.3–3.16 km), was comparatively less aerosol laden, with an AOD of 0.042 (±0.010) and a significantly higher PDR of 0.19–0.36, more consistent with Saharan dust or a dust/biomass burning mixture. In a second retrieval, slightly later, between 20:34 and 20:48 UTC (not shown) the upper layer was no longer present, and the lower layer was much less optically thick, but still with a PDR value comparable to that of air masses loaded with Saharan dust.

Two rain showers can be seen in the lidar data occurring just before 12:00 UTC and around 15:00 UTC, but with higher VDRs than those observed in precipitation events earlier in the day (*i.e.* region (ii) in Fig. 8b). This is likely a result of entraining smoke particles in the downdraught associated with the rain.

In the morning of the 16th October, the WCB was moving swiftly eastwards across the country, but by the afternoon its progress had slowed considerably as the associated cold front stalled over the UK. As such it took until ∼22:00 UTC for the Ophelia system to fully pass over Brighton and Hove and for the cold front to appear, in contrast to the report of Osborne *et al.*,[7] who observed the cold sector to appear as early as midday towards the western coast of the UK.

4 Conclusion: the *red sky*

The satellite observations presented here successfully provided a detailed, holistic 'snapshot' (from the 'top-down') of the Ophelia weather system with high spatial coverage but low temporal resolution. Used in concert with the orbital systems, the ground-based lidar provided complementary, near real-time information (from the 'bottom-up') on the types of particles entrained in the air mass as it slowed and passed over the UK.

By using top-down measurements from space it was possible to analyse the effect of the embedded aerosol on the light that was being scattered and subsequently the reddening of the Sun. Satellite measurements showed that the particle loading of the air mass was high, with an AI > 5, and contained significant levels of CO, up to almost 300 ppbV. By using bottom-up lidar measurements it was also possible to observe the temporal evolution, composition and the vertical extent of the aerosol–laden air mass. In combination with back-trajectory modelling, the satellite and ground-based measurements allowed the sources of the aerosol to be determined as Saharan dust uplift and wildfires across Portugal and Spain.

The lidar measurements showed that the *red sky* event comprised two distinct phases. The initial phase, observed between 00:00 and 10:00 UTC in the south of the UK was dominated by Saharan dust (VDR ~0.15–0.25; PDR ~0.27–0.42, where measurable), and the second phase, observed after 10:00 UTC contained an optically dense layer populated with a mixture of Saharan dust and biomass burning particles (VDR ~0.08–0.18; upper layer PDR ~0.10–0.13, lower layer PDR ~0.19–0.36, where measurable). It was this unique loading of aerosol types, rarely observed in this combination and magnitude over the UK, that resulted in enhanced scattering of the short/medium wavelengths of the incoming solar radiation, leading to the Sun and sky taking on a dramatic orangey, red appearance.

The findings reported from the Brighton and Hove lidar are consistent with, and supportive of those presented by Harrison *et al.*[5] and Osborne *et al.*,[7] which were based on data recorded earlier in the day and further to the east. Our findings also align with the CAMS modelling results presented by Moore,[6] which showed that the leading edge of the system carried a heavy loading of dust particles, and that this was followed by a distinct optically dense band containing biomass burning aerosol. Here we add to the small body of work that reports on this unique, 'perfect storm' of conditions and bring new lidar data and novel multispectral imaging to improve our understanding of what took place over the UK on the 16th October 2017. This work is not only important for the understanding of such unique weather phenomena, but also to help improve model accuracies for the medium to long-range transportation of aerosol in the lower atmosphere.

This study shows how an ensemble of 'top-down, bottom-up' measurements, using state-of-the-art space- and ground-based systems, and detailed modelling can be used to deconvolve complex atmospheric events and provide comprehensive insight into their origin, composition and evolution.

Data availability

NASA EOSDIS Worldview data is available at https://worldview.earthdata.nasa.gov. ESA Sentinel-2 data is available at https://scihub.copernicus.eu/. Lidar data is available on request to the corresponding author.

Author contributions

KPW, MB, HR and KLS designed the research. KPW and KLS were responsible for collecting the lidar data. KPW, HR, MB and KLS analysed the lidar data. MB conducted the Sentinel-2 MSI multispectral analysis. KPW conducted the NASA Worldview remote sensing and NOAA HYPSLIT back-trajectory modelling analysis. All authors contributed to writing and reviewing the manuscript.

Conflicts of interest

The authors declare that they have no conflict of interest.

Acknowledgements

The authors would like to thank Droplet Measurement Technologies and Enviro Technology Services Ltd for the loan of the MiniMPL-532-C elastic backscatter Mini Micro Pulse lidar system. Special thanks are given to Duncan Mounsor of Enviro Technology Services Ltd for leading on the loan and for the setting up of the lidar system. We acknowledge the use of imagery from the NASA Worldview application (https://worldview.earthdata.nasa.gov), part of the NASA Earth Observing System Data and Information System (EOSDIS). We also acknowledge the use of Copernicus Sentinel data 2017, retrieved from the Copernicus Open Access Hub (https://scihub.copernicus.eu) [01/12/2018], processed by ESA. The authors acknowledge the VIIRS, MODIS, OMI, AIRS and MSI mission scientists and associated personnel for the production of the respective satellite data.

References

1 B. J. Finlayson-Pitts and J. N. Pitts Jr, *Chemistry of the upper and lower atmosphere: theory, experiments, and applications*, Elsevier, 1999, DOI: 10.1016/b978-0-12-257060-5.x5000-x.

2 X. Yang, C. Zhao, L. Zhou, Y. Wang and X. Liu, Distinct impact of different types of aerosols on surface solar radiation in China, *J. Geophys. Res.: Atmos.*, 2016, **121**(11), 6459–6471, DOI: 10.1002/2016jd024938.

3 X. Yang, C. Zhao, L. Zhou, Z. Li, M. Cribb and S. Yang, Wintertime cooling and a potential connection with transported aerosols in Hong Kong during recent decades, *Atmos. Res.*, 2018, **211**, 52–61, DOI: 10.1016/j.atmosres.2018.04.029.

4 G. S. Smith, Human color vision and the unsaturated blue color of the daytime sky, *Am. J. Phys.*, 2005, **73**(7), 590–597.

5 R. G. Harrison, K. A. Nicoll, G. J. Marlton, C. L. Ryder and A. J. Bennett, Saharan dust plume charging observed over the UK, *Environ. Res. Lett.*, 2018, **13**(5), 054018.

6 D. P. Moore, The October 2017 red sun phenomenon over the UK, *Weather*, 2019, **74**(10), 348–353.

7 M. Osborne, F. F. Malavelle, M. Adam, J. Buxmann, J. Sugier, F. Marenco and J. Haywood, Saharan dust and biomass burning aerosols during ex-hurricane Ophelia: observations from the new UK lidar and sun-photometer network, *Atmos. Chem. Phys.*, 2019, **19**(6), 3557–3578.

8 O. Boucher, *Atmospheric Aerosols*, Springer, Dordrecht, 2015, pp. 9–24.

9 D. Camuffo and S. Enzi, Impact of the clouds of volcanic aerosols in Italy during the last 7 centuries, *Nat. Hazards*, 1995, **11**(2), 135–161.

10 V. V. Salomonson, W. L. Barnes, P. W. Maymon, H. E. Montgomery and H. Ostrow, MODIS: Advanced facility instrument for studies of the Earth as a system, *IEEE Trans. Geosci. Remote Sens.*, 1989, **27**(2), 145–153.

11 C. Cao, F. J. De Luccia, X. Xiong, R. Wolfe and F. Weng, Early on-orbit performance of the visible infrared imaging radiometer suite onboard the Suomi National Polar-Orbiting Partnership (S-NPP) satellite, *IEEE Trans. Geosci. Remote Sens.*, 2013, **52**(2), 1142–1156.

12 A. M. Sayer, N. C. Hsu, C. Bettenhausen, J. Lee, W. V. Kim and A. Smirnov, Satellite Ocean Aerosol Retrieval (SOAR) Algorithm Extension to S-NPP VIIRS as Part of the "Deep Blue" Aerosol Project, *J. Geophys. Res.: Atmos.*, 2018, **123**, 380–400, DOI: 10.1002/2017jd027412.

13 W. Schroeder, P. Oliva, L. Giglio and I. A. Csiszar, The New VIIRS 375m active fire detection data product: algorithm description and initial assessment, *Remote Sens. Environ.*, 2014, **143**, 85–96, DOI: 10.1016/j.rse.2013.12.008.

14 H. H. Aumann, M. T. Chahine, C. Gautier, M. D. Goldberg, E. Kalnay, L. M. McMillin, H. Revercomb, P. W. Rosenkranz, W. L. Smith, D. H. Staelin and L. L. Strow, AIRS/AMSU/HSB on the Aqua mission: design, science objectives, data products, and processing systems, *IEEE Trans. Geosci. Remote Sens.*, 2003, **41**(2), 253–264.

15 O. Torres, Z. Chen, H. Jethva, C. Ahn, S. R. Freitas and P. K. Bhartia, OMI and MODIS observations of the anomalous 2008–2009 Southern Hemisphere biomass burning seasons, *Atmos. Chem. Phys.*, 2010, **10**, 3505–3513, DOI: 10.5194/acp-10-3505-2010.

16 P. F. Levelt, G. H. J. van den Oord, M. R. Dobber, A. Mälkki, H. Visser, J. de Vries, P. Stammes, J. Lundell and H. Saari, The Ozone Monitoring Instrument, *IEEE Trans. Geosci. Remote Sens.*, 2006, **44**(5), 1093–1101, DOI: 10.1109/tgrs.2006.872333.

17 A. J. Adesina, K. R. Kumar, V. Sivakumar and S. J. Piketh, Intercomparison and assessment of long-term (2004–2013) multiple satellite aerosol products over two contrasting sites in South Africa, *J. Atmos. Sol.-Terr. Phys.*, 2016, **148**, 82–95, DOI: 10.1016/j.jastp.2016.09.001, ISSN:1364-6826.

18 KNMI, *UV Aerosol Optical Depth and Single Scattering Albedo data (OMAERUV)*, 2020, available at: http://projects.knmi.nl/omi/research/product/product_generator.php?info=intro&product=aerosol.

19 M. Drusch, U. Del Bello, S. Carlier, O. Colin, V. Fernandez, F. Gascon, B. Hoersch, C. Isola, P. Laberinti, P. Martimort and A. Meygret, Sentinel-2: ESA's optical high-resolution mission for GMES operational services, *Remote Sens. Environ.*, 2012, **120**, 25–36.

20 R. Gautam, C. K. Gatebe, M. K. Singh, T. Várnai and R. Poudyal, Radiative characteristics of clouds embedded in smoke derived from airborne multiangular measurements, *J. Geophys. Res.: Atmos.*, 2016, **121**(15), 9140–9152, DOI: 10.1002/2016jd025309.

21 B. C. Gao, W. Han, S. C. Tsay and N. F. Larsen, Cloud detection over the Arctic region using airborne imaging spectrometer data during the daytime, *J. Appl. Meteorol.*, 1998, **37**(11), 1421–1429, DOI: 10.1175/1520-0450(1998)037<1421:CDOTAR>2.0.CO;2.

22 P. Stammes, J. R. Acarreta, W. H. Knap and L. G. Tilstra, Earth reflectance spectra from 300–1750 nm measured by SCIAMACHY, in *Current Problems in Atmospheric Radiation, International Radiation Symposium*, Hampton, Busan, Korea, 2004, pp. 215–218.

23 J. J. Qu, X. Hao, M. Kafatos and L. Wang, Asian dust storm monitoring combining Terra and Aqua MODIS SRB measurements, *IEEE Trans. Geosci. Remote Sens.*, 2006, **3**(4), 484–486.

24 S. H. Park, M. J. Lee and H. S. Jung, Analysis on the snow cover variations at Mt. Kilimanjaro using Landsat satellite images, *Korean J. Remote Sens.*, 2012, **28**(4), 409–420, DOI: 10.7780/kjrs.2012.28.4.5.

25 J. D. Spinhirne, Micro pulse lidar, *IEEE Trans. Geosci. Remote Sens.*, 1993, **31**(1), 48–55.

26 T. F. Eck, B. N. Holben, J. S. Reid, A. Arola, R. A. Ferrare, C. A. Hostetler, S. N. Crumeyrolle, T. A. Berkoff, E. J. Welton, S. Lolli and A. Lyapustin, Observations of rapid aerosol optical depth enhancements in the vicinity of polluted cumulus clouds, *Atmos. Chem. Phys.*, 2014, **14**(21), 11633–11656.

27 F. Höpner, F. M. Bender, A. M. Ekman, P. S. Praveen, C. Bosch, J. A. Ogren, A. Andersson, Ö. Gustafsson and V. Ramanathan, Vertical profiles of optical and microphysical particle properties above the northern Indian Ocean during CARDEX 2012, *Atmos. Chem. Phys.*, 2016, **16**(2), 1045–1064.

28 W. B. Johnson, Lidar applications in air pollution research and control, *J. Air Pollut. Control Assoc.*, 1969, **19**(3), 176–180.

29 F. Cairo, G. Donfrancesco, A. Adriani, L. Pulvirenti and F. Federico, Comparison of various linear depolarization parameters measured by lidar, *Appl. Opt.*, 1999, **38**, 4425–4432.

30 T. Murayama, D. Müller, K. Wada, A. Shimizu, M. Sekiguchi and T. Tsukamoto, Characterization of Asian dust and Siberian smoke with multi-wavelength Raman lidar over Tokyo, Japan in spring 2003, *Geophys. Res. Lett.*, 2004, **31**, L23103, DOI: 10.1029/2004gl021105.

31 J. D. Klett, Stable analytical inversion solution for processing lidar returns, *Appl. Opt.*, 1981, **20**(2), 211–220.

32 F. G. Fernald, Analysis of atmospheric lidar observations: some comments, *Appl. Opt.*, 1984, **23**(5), 652–653, DOI: 10.1364/ao.23.000652.

33 V. Freudenthaler, M. Esselborn, M. Wiegner, B. Heese, M. Tesche, A. Ansmann, D. Müller, D. Althausen, M. Wirth, A. Fix and G. Ehret, Depolarization ratio profiling at several wavelengths in pure Saharan dust during SAMUM 2006, *Tellus B*, 2009, **61**(1), 165–179.

34 A. Behrendt and T. Nakamura, Calculation of the calibration constant of polarization lidar and its dependency on atmospheric temperature, *Opt. Express*, 2002, **10**(16), 805–817.

35 L. Solari, M. Del Soldato, S. Bianchini, A. Ciampalini, P. Ezquerro, R. Montalti, F. Raspini and S. Moretti, From ERS 1/2 to Sentinel-1: Subsidence Monitoring in Italy in the Last Two Decades, *Front. Earth Sci.*, 2018, **6**, DOI: 10.3389/feart.2018.00149.

36 S. Burns, *Ireland's highest wind gust recorded during Storm Ophelia*, 2017, The Irish Times, 05/12/2017, available at: https://www.irishtimes.com/news/environment/ireland-s-highest-wind-gust-recorded-during-storm-ophelia-1.3316270, accessed: 03/03/2021.

37 A. F. Stein, R. R. Draxler, G. D. Rolph, B. J. Stunder, M. D. Cohen and F. Ngan, NOAA's HYSPLIT atmospheric transport and dispersion modeling system, *Bull. Am. Meteorol. Soc.*, 2015, **96**(12), 2059–2077.

38 G. Pace, A. D. Sarra, D. Meloni, S. Piacentino and P. Chamard, Aerosol optical properties at Lampedusa (Central Mediterranean). 1. Influence of transport and identification of different aerosol types, *Atmos. Chem. Phys.*, 2006, **6**(3), 697–713.

39 M. Tesche, A. Ansmann, D. Müller, D. Althausen, R. Engelmann, V. Freudenthaler and S. Groß, Vertically resolved separation of dust and smoke over Cape Verde using multiwavelength Raman and polarization lidars during Saharan Mineral Dust Experiment 2008, *J. Geophys. Res.: Atmos.*, 2009, **114**, D13202, DOI: 10.1029/2009jd011862.

40 C. D. O'Dowd and M. H. Smith, Physicochemical properties of aerosols over the northeast Atlantic: evidence for wind-speed-related submicron sea-salt aerosol production, *J. Geophys. Res.: Atmos.*, 1993, **98**(D1), 1137–1149.

41 M. O. Andreae and P. Merlet, Emission of trace gases and aerosols from biomass burning, *Global Biogeochem. Cycles*, 2001, **15**(4), 955–966.

42 P. Guyon, G. P. Frank, M. Welling, D. Chand, P. Artaxo, L. Rizzo, G. Nishioka, O. Kolle, H. Fritsch, S. Dias and L. V. Gatti, Airborne measurements of trace gas and aerosol particle emissions from biomass burning in Amazonia, *Atmos. Chem. Phys.*, 2005, **5**(11), 2989–3002.

43 J. Brito, L. V. Rizzo, W. T. Morgan, H. Coe, B. Johnson, J. Haywood, K. Longo, S. Freitas, M. O. Andreae and P. Artaxo, Ground-based aerosol characterization during the South American Biomass Burning Analysis (SAMBBA) field experiment, *Atmos. Chem. Phys.*, 2014, **14**(22), 2069–12083.

44 M. O. Andreae, Emission of trace gases and aerosols from biomass burning – an updated assessment, *Atmos. Chem. Phys.*, 2019, **19**(13), 8523–8546.

45 X. Yang, C. Zhao, Y. Yang and H. Fan, Long-term multi-source data analysis about the characteristics of aerosol optical properties and types over Australia, *Atmos. Chem. Phys.*, 2021, **21**(5), 3803–3825, DOI: 10.5194/acp-21-3803-2021.

46 X. Yang, C. Zhao, Y. Yang, X. Yan and H. Fan, Statistical aerosol properties associated with fire events from 2002 to 2019 and a case analysis in 2019 over Australia, *Atmos. Chem. Phys.*, 2021, **21**(5), 3833–3853, DOI: 10.5194/acp-21-3833-2021.

47 BBC, *Indonesia haze causes sky to turn blood red*, 2019, BBC News, 23/09/2019, available at: https://www.bbc.co.uk/news/world-asia-49793047, accessed 18/03/2021.

48 D. Bliss, *British wildfires are getting more frequent. Here's what that means*, 2020, Natl. Geogr., 27/04/2020, available at: https://www.nationalgeographic.co.uk/environment-and-conservation/2020/04/british-wildfires-are-getting-more-frequent-heres-what-that, accessed 18/03/2021.

49 A. Mckeever, Foreboding orange skies cast more than a pall over Northern California, Natl. Geogr., 10/09/2020, September 10, 2020, available at: https://www.nationalgeographic.com/science/article/foreboding-orange-skies-cast-more-than-pall-over-northern-california, accessed 18/03/2021.

50 K. Paul, *Good morning, hell': Californians awake to apocalyptic skies as wildfires rage*, The Guardian, 09/09/2020, Wed 9 Sep 2020 , available at: https://www.theguardian.com/us-news/2020/sep/09/orange-sky-california-fires-smoke-san-francisco, accessed 18/03/2021.

51 A. S. Goudie and N. J. Middleton, Saharan dust storms: nature and consequences, *Earth-Sci. Rev.*, 2001, **56**(1–4), 179–204.

52 A. Cuspilici, P. Monforte and M. A. Ragusa, Study of Saharan dust influence on PM10 measures in Sicily from 2013 to 2015, *Ecol. Indic.*, 2017, **76**, 297–303.

53 K. Dimitriou and P. Kassomenos, Estimation of North African dust contribution on PM10 episodes at four continental Greek cities, *Ecol. Indic.*, 2019, **106**, 105530.

54 F. Oduber, A. I. Calvo, C. Blanco-Alegre, A. Castro, T. Nunes, C. Alves, M. Sorribas, D. Fernández-González, A. M. Vega-Maray, R. M. Valencia-Barrera and F. Lucarelli, Unusual winter Saharan dust intrusions at Northwest Spain: Air quality, radiative and health impacts, *Sci. Total Environ.*, 2019, **669**, 213–228.

55 H. Liu, L. A. Remer, J. Huang, H. C. Huang, S. Kondragunta, I. Laszlo, M. Oo and J. M. Jackson, Preliminary evaluation of S-NPP VIIRS aerosol optical thickness, *J. Geophys. Res.: Atmos.*, 2014, **119**(7), 3942–3962.

56 F. Meng, C. Cao and X. Shao, Spatio-temporal variability of Suomi-NPP VIIRS-derived aerosol optical thickness over China in 2013, *Remote Sens. Environ.*, 2015, **163**, 61–69.

57 C. Li, J. Li, H. Xu, Z. Li, X. Xia and H. Che, Evaluating VIIRS EPS Aerosol Optical Depth in China: An intercomparison

against ground-based measurements and MODIS, *J. Quant. Spectrosc. Radiat. Transfer*, 2019, **224**, 368–377.

58 Y. Yang, C. Zhao, L. Sun and J. Wei, Improved aerosol retrievals over complex regions using NPP Visible Infrared Imaging Radiometer Suite observations, *Earth and Space Science*, 2019, **6**(4), 629–645, DOI: 10.1029/2019ea000574.

59 P. L. Israelevich, Z. Levin, J. H. Joseph and E. Ganor, Desert aerosol transport in the Mediterranean region as inferred from the TOMS aerosol index, *J. Geophys. Res.: Atmos.*, 2002, **107**(D21), AAC-13.

60 W. W. McMillan, J. X. Warner, M. M. Comer, E. Maddy, A. Chu, L. Sparling, E. Eloranta, R. Hoff, G. Sachse, C. Barnet and I. Razenkov, AIRS views transport from 12 to 22 July 2004 Alaskan/Canadian fires: Correlation of AIRS CO and MODIS AOD with forward trajectories and comparison of AIRS CO retrievals with DC-8 *in situ* measurements during INTEX-A/ICARTT, *J. Geophys. Res.: Atmos.*, 2008, **113**, D20301, DOI: 10.1029/2007jd009711.

61 S. K. Kharol, K. V. S. Badarinath and P. S. Roy, Studies on emissions from forest fires using multi-satellite datasets over north east region of India, The international archives of the society for photogrammetry and remote sensing, *ISPRS Archives*, 2008, vol. 37.

62 O. Torres, Z. Chen, H. Jethva, C. Ahn, S. R. Freitas and P. K. Bhartia, OMI and MODIS observations of the anomalous 2008–2009 Southern Hemisphere biomass burning seasons, *Atmos. Chem. Phys.*, 2010, **10**(8), 3505–3513.

63 J. M. Rajab, K. C. Tan, H. S. Lim and M. Z. Mat Jafri, Investigation on the carbon monoxide pollution over Peninsular Malaysia caused by Indonesia forest fires from AIRS daily measurement, in *Advanced Air Pollution*, ed. F. Nejadkoorki, InTech, Croatia, 2011, ch. 8, pp. 115–136.

64 R. D. Field, G. R. Van Der Werf, T. Fanin, E. J. Fetzer, R. Fuller, H. Jethva, R. Levy, N. J. Livesey, M. Luo, O. Torres and H. M. Worden, Indonesian fire activity and smoke pollution in 2015 show persistent nonlinear sensitivity to El Niño-induced drought, *Proc. Natl. Acad. Sci. U. S. A.*, 2016, **113**(33), 9204–9209.

65 R. Gautam, N. C. Hsu, T. F. Eck, B. N. Holben, S. Janjai, T. Jantarach, S. C. Tsay and W. K. Lau, Characterization of aerosols over the Indochina peninsula from satellite-surface observations during biomass burning pre-monsoon season, *Atmos. Environ.*, 2013, **78**, 51–59.

66 J. Huang, P. Minnis, Y. Yi, Q. Tang, X. Wang, Y. Hu, Z. Liu, K. Ayers, C. Trepte and D. Winker, Summer dust aerosols detected from CALIPSO over the Tibetan Plateau, *Geophys. Res. Lett.*, 2007, **34**(18), L18805, DOI: 10.1029/2007gl029938.

67 Z. Liu, D. Liu, J. Huang, M. Vaughan, I. Uno, N. Sugimoto, C. Kittaka, C. Trepte, Z. Wang, C. Hostetler and D. Winker, Airborne dust distributions over the Tibetan Plateau and surrounding areas derived from the first year of CALIPSO lidar observations, *Atmos. Chem. Phys.*, 2008, **8**(16), 5045–5060.

68 M. Haarig, A. Ansmann, D. Althausen, A. Klepel, S. Groß, V. Freudenthaler, C. Toledano, R. E. Mamouri, D. A. Farrell, D. A. Prescod and E. Marinou, Triple-wavelength depolarization-ratio profiling of Saharan dust over Barbados during SALTRACE in 2013 and 2014, *Atmos. Chem. Phys.*, 2017, **17**(17), 10767–10794.

69 A. J. Illingworth, H. W. Barker, A. Beljaars, M. Ceccaldi, H. Chepfer, N. Clerbaux, J. Cole, J. Delanoë, C. Domenech, D. P. Donovan and S. Fukuda, The EarthCARE satellite: the next step forward in global measurements of clouds, aerosols, precipitation, and radiation, *Bull. Am. Meteorol. Soc.*, 2015, **96**(8), 1311–1332.

70 S. Groß, M. Tesche, V. Freudenthaler, C. Toledano, M. Wiegner, A. Ansmann, D. Althausen and M. Seefeldner, Characterization of Saharan dust, marine aerosols and mixtures of biomass-burning aerosols and dust by means of multi-wavelength depolarization and Raman lidar measurements during SAMUM 2, *Tellus B*, 2011, **63**(4), 706–724.

71 Y. X. Hu, D. Winker, P. Yang, B. Baum, L. Poole and L. Vann, Identification of cloud phase from PICASSO-CENA lidar depolarization: a multiple scattering sensitivity study, *J. Quant. Spectrosc. Radiat. Transfer*, 2001, **70**(4–6), 569–579.

72 G. Roy and N. Roy, Relation between circular and linear depolarization ratios under multiple-scattering conditions, *Appl. Opt.*, 2008, **47**(35), 6563–6579.

73 Z. Zhang, J. Huang, B. Chen, Y. Yi, J. Liu, J. Bi, T. Zhou, Z. Huang and S. Chen, Three-year continuous observation of pure and polluted dust aerosols over Northwest China using the ground-based lidar and sun photometer data, *J. Geophys. Res.: Atmos.*, 2019, **124**(2), 1118–1131.

74 Y. Tian, X. Pan, Z. Wang, D. Wang, B. Ge, X. Liu, Y. Zhang, H. Liu, S. Lei, T. Yang and P. Fu, Transport Patterns, Size Distributions, and Depolarization Characteristics of Dust Particles in East Asia in Spring 2018, *J. Geophys. Res.: Atmos.*, 2020, **125**(16), e2019JD031752.

75 G. Vaughan, D. Wareing and H. Ricketts, Measurement Report: Lidar measurements of stratospheric aerosol following the Raikoke and Ulawun volcanic eruptions, *Atmos. Chem. Phys. Discuss.*, 2020, 1–10.

76 S. Groß, V. Freudenthaler, M. Wirth and B. Weinzierl, Towards an aerosol classification scheme for future EarthCARE lidar observations and implications for research needs, *Atmospheric Sci. Lett.*, 2015, **16**, 77–82, DOI: 10.1002/asl2.524.